Fast Localization of Optic Disc and Fovea in Retinal Images for Eye Disease Screening

H Yu*[a,b], S Barriga[b], C Agurto[a,b], S Echegaray[b], M Pattichis[a], G Zamora[b], W Bauman[c] and P Soliz[b]
[a] VisionQuest Biomedical, Albuquerque, NM, USA 87106
[b]Dept. of Electrical& Computer Engineering, Univ. of New Mexico, Albuquerque, NM, USA87131
[c] Retina Institute of South Texas, San Antonio, TX, USA 78233

ABSTRACT

Optic disc (OD) and fovea locations are two important anatomical landmarks in automated analysis of retinal disease in color fundus photographs. This paper presents a new, fast, fully automatic optic disc and fovea localization algorithm developed for diabetic retinopathy (DR) screening. The optic disc localization methodology comprises of two steps. First, the OD location is identified using template matching and directional matched filter. To reduce false positives due to bright areas of pathology, we exploit vessel characteristics inside the optic disc. The location of the fovea is estimated as the point of lowest matched filter response within a search area determined by the optic disc location. Second, optic disc segmentation is performed. Based on the detected optic disc location, a fast hybrid level-set algorithm which combines the region information and edge gradient to drive the curve evolution is used to segment the optic disc boundary. Extensive evaluation was performed on 1200 images (Messidor) composed of 540 images of healthy retinas, 431 images with DR but no risk of macular edema (ME), and 229 images with DR and risk of ME. The OD location methodology obtained 98.3% success rate, while fovea location achieved 95% success rate. The average mean absolute distance (MAD) between the OD segmentation algorithm and "gold standard" is 10.5% of estimated OD radius. Qualitatively, 97% of the images achieved Excellent to Fair performance for OD segmentation. The segmentation algorithm performs well even on blurred images.

Keywords: retinal imaging, optic disc, fovea, segmentation, deformable model, level sets, diabetic retinopathy.

1. INTRODUCTION

1.1 Motivation

Diabetic Retinopathy (DR) is a retinal disease caused by complications of diabetes mellitus, which can eventually lead to blindness. Prior to the onset of perceived visual loss, DR patients may not present any symptoms. If DR is detected early, the treatment is more effective and significant savings in care costs can be realized.

Automated retinal image analysis promises to provide objective, fast, accurate, and consistent screening information to augment manual screening of the growing diabetic population. One of the first requirements for automatic screening of DR is the localization of anatomical landmarks such as the optic disc, fovea, and retinal vasculature.

The optic disc center and margin are typically requisite landmarks in establishing a frame of reference for classifying retinal pathology. The optic disc is the region of the retina where the vasculature enters and leaves the eye and its appearance is different from the surrounding retinal tissue. The optic disc in a healthy retinal image usually appears as a bright yellowish and ellipse-shaped object marked by vessels. However, the entire retina as well as the optic disc may appear different due to the natural geometry of the scene or technical errors in the photography. A retina image may, for instance, suffer uneven illumination resulting in a less distinct and blurred appearance of OD. The temporal side of optic disc is usually brighter than the nasal side (in macula-centered photographs). Retinal abnormalities may also dramatically affect the appearance of the OD. Image examples exhibiting large variations in the appearance of the optic disc are shown in Figure 1. During the development of an automatic OD localization method it is important to consider that the optic disc variations in appearance, size and location.

*hyu@visionquest-bio.com; phone 505.508.1994; fax 505.508.5308; http://visionquest-bio.com/index.html

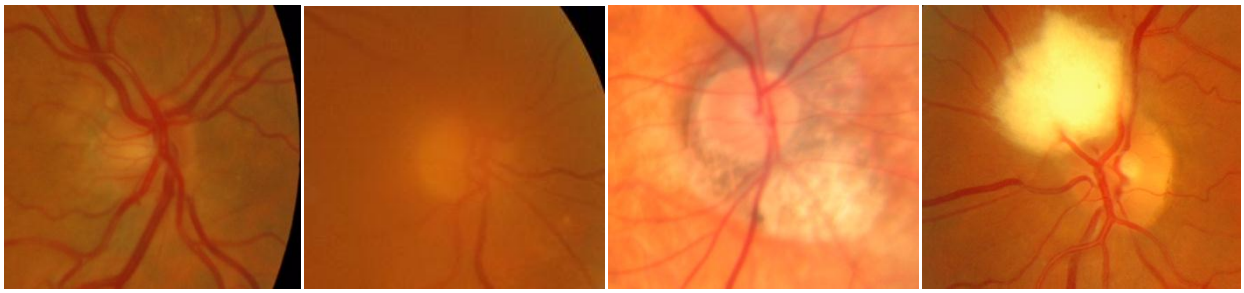

(a) (b) (c) (d)

Figure. 1 Diverse appearance of the optic disc. (a) Uneven OD brightness with distinct large vessels (b) Blurred OD appearance caused by cataract (c) OD appearance with peripapillary atrophy (d) Myelinated nerve fibers connected to OD margin

1.2 Optic disc location state of the art

A number of different techniques have been employed to automatically detect the optic disc. Reviews of OD detection methods were given by Winder, et al. [1] (for all image processing steps in diabetic retinopathy) and Youssif [2] (specially for optic disc detection). Osareh, et al. used template matching based on high intensity and shape [3]. Lalonde, et al. developed pyramidal decomposition with Hausdorff-based template matching [4]. Lowell, et al. used template matching to locate OD and initialize OD segmentation, which was performed using a global elliptical shape model combined with local variable stiffness model [5]. State-of-the-art OD localization techniques not only use the characteristics of OD, but also exploit the location and orientation of vessels [6-9]; Hoover, et al. applied fuzzy convergence of blood vessels to locate the center of OD [10]. Foracchia, et al. localizes the OD by fitting a parametric geometrical model to the main vessels extracted from the image [11]. The use of the vasculature could improve the OD localization reliability, especially when OD is not visible within the image. On the other hand, the prerequisite step of segmenting the vascular tree to detect OD is a complex and difficult task. Its performance is affected by bright lesions and the OD contour. Misclassification of the vasculature may degrade the performance of subsequent OD detection.

Our purpose is to develop a fast, efficient and robust algorithm for OD localization in DR screening. We use vessel characteristics inside the OD region to aid in this task. Our method uses template matching in the CIELab lightness image to select OD candidates. Further identification of the OD location is implemented by directional matched filter in the green channel within the OD candidates. This methodology not only quickly exploits the high intensity, large intensity variation and elliptical shape of optic disc, but also utilizes vessel characteristics inside optic disc.

Temporal to the optic disc is the pigmented macula which appears darker in color. The avascular fovea lies at the center of the macula and is the part of the retina that is used for fine vision. The macula is an approximately circular dark area, but the contrast is often quite low and it may be obscured somewhat by exudates and hemorrhages. The fovea is located approximately 2–2.5 disc diameters to the temporal edge of the optic disc and between the major temporal retinal vascular arches. These positional constraints can be used to identify a small search area for the fovea. The location with the lowest template matching response within the fovea search region is selected as the fovea location.

1.3 Optic disc segmentation state of the art

Previous investigators have described a variety of algorithms for the OD boundary segmentation. Active contours is one of the most promising approaches in this area. Mendels, et al. [12] investigated applying a morphological operator followed by the GVF active contour to segment the disk with an interactively initialized curve which is set close to the true contour of OD. The technique was tested on a set of nine retinal images but no quantitative evaluation was presented. Osareh, et al. [3] has proposed intensity template matching to initialize the deform contour. Then they used color morphological processing to obtain a more homogeneous inner disc area, which increased the accuracy of the GVF active contour segmentation. An overall accuracy of 91.84% was reported in comparison to the reference standard of a clinical ophthalmologist on 75 images. Lowell, et al. [5] also first localized OD by a template matching technique. A global elliptical parametric model combined with local variable edge-strength dependent stiffness model was then fitted to the contour of the disk. The algorithm was evaluated on 90 over 100 images since 10 images were classified as unusable. The algorithm achieved excellent-fair performance in 83% of cases. Li [13] proposed a modified active shape

model (ASM) to segment OD for exudates detection. The algorithm successfully detected the OD boundary in 33 of 35 images. OD boundary segmentation is an essential procedure for glaucoma analysis. Xu [14] proposed an improved deformable model by using knowledge-based clustering and smoothing update to reduce false deformation in OD and cup segmentation. The proposed method achieved 94% success rate for the 100 images. The above researches were conducted on a limited number of retinal images. The performance of those algorithms could be significantly degraded if applied to a large number of images exhibiting a significant variation in the OD appearance due to imaging quality, retinal lesions and other artifacts. Recently, Aquino [15] presented a fast OD boundary detection technique and evaluated on Messidor database, which consists of 1200 retinal images. The segmentation was performed in parallel on both red channel and green channel of the down-sampled images. The channel with the higher score in the circular Hough transform based on the edge map is selected as the OD boundary approximation. Compared to the above algorithms, our OD detection algorithm exploits vessel characteristics inside OD besides the template matching. All the parameters of template and image processing parameters are set automatically base on the size of field of view of camera. Our OD segmentation algorithm deform the evolving curve based on the region intensity and edge vector, which performs very well on blurred OD. No special requirement for curve initialization is needed in our method. The curve automatically deforms to the OD boundary based on automatically set region threshold. All the processes are performed on the original image, without image size scaling, which inevitably loses image information for the processing.

2. METHODOLOGY

2.1 Optic disc and fovea detection algorithm

The optic disc location algorithm is designed based on the characteristics of the different channels in digital color fundus images. Although in the red channel of fundus images the optic disc generally has good intensity contrast and well-defined boundaries, this observation is not always true in diabetic retinopathy images. Even in healthy retinal images, red channel image saturation is common due to the imaging technique or eye/fundus pigmentation.

CIElab is the most complete color space specified by the International Commission on Illumination. It is designed to approximate human vision and serve as a device independent model to be used as a reference. Its lightness component L closely matches human perception. In the L component image of CIELab color space, the optic disc keeps good intensity contrast and well-defined boundaries. Meanwhile, the image lightness is more uniform and less saturated than the one in the red channel. Our experiments verified that template matching in CIElab L component images has a better performance than in red channel images.

A description of the detection algorithm, as well as an example of the algorithm applied to a diabetic retinopathy fundus image (Figure 2), is presented as follows. A region-of-interest (ROI) mask is generated to separate the pixels that belong to the field of view (FOV) from the background after converting the RGB color image to CIElab color space. All the sequential steps were performed in the FOV mask.

Template matching

A binary template consists of a white disk with value 1 and black background with value 0 is used instead of averaging multiple retinal images to generate the template (Figure 2(a)). The performance of this simple template is not inferior compared to the intensity template. We have experimented with the usage of a few variations of the template, and concluded that there are no significant advantages in using a specific one. The radius of the white circle is determined based on an estimate of the optic disc diameter. The size of the optic disc varies significantly in different images. The images in the Messidor database are acquired using a color video 3CCD camera on a Topcon TRC NW6 non-mydriatic retinograph with a 45 degree field of view. The imaged area of the retina is 124.8 mm^2 for a 45 degree FOV [16]. We can formulate the computation of OD diameter in an image (pixels) based on the diameter of the average optic nerve head (d_{OD}) , which is assumed to be approximately 1850 μm in the eye [17].

In the FOV mask, we can count the number of pixels N_{FOV} in the FOV. Then, the image footprint is computed as:

$$f_{img} = A_{FOV}/N_{FOV}$$

where, A_{FOV} is the imaged area of the specific field of view. Then we can compute the OD diameter in pixels d_{OD_img} using the average area size of optic nerve head A_{OD} and the image footprint:

$$d_{OD\_img} = 2 \times \sqrt{\frac{(A_{OD}/f_{img})}{\pi}} = \sqrt{\frac{{d_{OD}}^2}{f_{img}}}$$

where $A_{OD} = \pi(d_{OD}/2)^2$.

Then all the template parameters are determined automatically based on the estimated OD diameter or OD radius. The template length is set to be 3 times the OD radius. Since the purpose of template matching is only to coarsely search the OD candidates, we speed up the algorithm by setting search distance as one fourth of the OD radius.

The Pearson correlation coefficient is used to measure the degree to which CIElab lightness sub-image and template agree in general behavior. The template matching responses were sorted in ranked order. The same values need to be in the same rank to ensure selecting all the possible OD candidates. The locations of a certain percentage of the largest template matching responses were selected as OD candidates (Figure 2, (c)).

Directional matched filtering

The use of directional matched filtering in OD candidates is to distinguish the real OD location, where vertical vessels pass through, from the large bright regions, such as exudates, myelinated nerve fibers etc. The intensity profile of the cross section of a retinal vessel can be approximated by a Gaussian shaped curve. The two dimensional matched filter kernel is designed to convolve with the green channel image in order to enhance and detect the vessels inside OD candidates[18]. A prototype matched filter kernel, which matching a number of cross sections along vessel length is expressed as

$$G(x,y) = -a\, e^{-x^2/2\sigma^2}, for\ |y| \le L/2$$

where L is the length of the segment for which the vessel is assumed to have a fixed orientation ($L = 9$). The direction of the vessel is assumed to be aligned along the *y* axis. Since the vessels inside the OD region appear nearly along the vertical direction, the Gaussian kernel (15×16 pixels) used here is along the horizontal profile. The vessel width inside OD normally is 15% of the OD diameter [19]. We found that the maximal vessel width is 13 pixels from the above OD diameter computation for all the images in Messidor database. Within the OD candidates, only the vertical vessels are enhanced by the directional matched filtering. The candidate with the maximum standard deviation after matched filtering in the region is determined to be the OD location (Figure 2 (d)).

Fovea detection

The fovea is located approximately 2–2.5 optic disc diameters away from the temporal edge of the optic disc. Based on the detected optic disc location two fovea search regions are defined. One for the case the image is obtained from the left eye and one for the right eye case. In the left eye fundus image the fovea is located to the right of the optic disc and vice versa for the right eye fundus image. As it is unknown a priori whether the image is for left or right eye, both search regions need to be considered. We can always exclude one search region that falls outside of the FOV. The search region has been defined as follows: we choose the center of the search region as the location which is at 4.5 times OD radius to the optic disc. The search region is a square with length of 2 disc diameters (blue square, Figure 2 (d)). No further template matching computation is needed, since the template matching responses in OD detection were saved and the minimum response to the template matching in the fovea search region is the location of fovea.

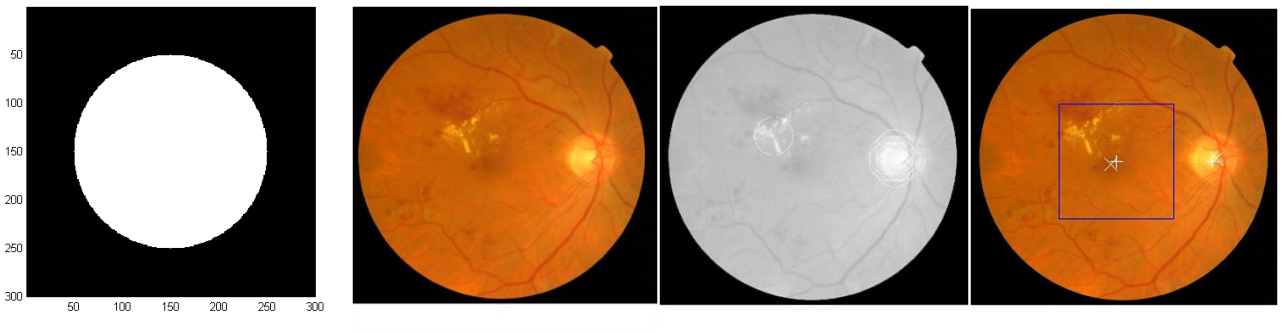

(a) (b) (c) (d)

Figure 2. OD and fovea detection (a) Template (b) A retinal image with grade 3 DR and grade 2 risk of ME. (b) OD candidates after template matching in the CIELab Lchannel. (c) OD and fovea location result (X is the ground truth, + is the detected OD and fovea location).

2.2 Optic disc segmentation algorithm

In some cases, the optic disc boundary may appear blurred and faint due to cataract or inadequate photography, or the vessels obscure the OD margins. We use a fast hybrid level set model [20] with automatic initialization to solve this difficulty in OD segmentation. This model uses the region intensity information and edge vector to drive the deformable contour converges to the true OD boundary. The OD segmentation is performed on a cropped sub-image, centered at the detected OD location, the size of the ROI is $3d_{OD\_img} \times 3d_{OD\_img}$. The initial contour can be automatically set as a circle with the center at the detected OD location and the radius equal the estimated OD radius.

Saturation Detection in Red Channel

Having compared several color spaces, we found that the OD appear most contrasted against the background and has least vessel distractions in the red channel. Our OD segmentation is performed in red channel. But in some images, the red channel is saturated around the OD that degraded the algorithm performance. For the images, whose red channels are saturated, CIELab lightness image is used for OD segmentation. A red channel saturation detection algorithm was developed based on the red channel intensity information in ROI region.

We have $r_{OD\_img} = d_{OD\_img}/2$, then the OD area $A_{OD\_img} = \pi {r_{OD\_img}}^2$, the ROI area is $A_{ROI} = 36{r_{OD\_img}}^2$. The OD occupies about one-tenth of the ROI sub-image. This means that the 90th percentile value approaches the maximum intensity value in the ROI. If the red channel is saturated, there are a lot of bright pixels in the ROI, thus we check that if the 50th percentile value in ROI is larger than 80% of the maximum intensity value, then the OD segmentation is performed in CIElab image instead of the red channel.

Vessel Removal

Because blood vessels introduce errors in OD segmentation, they must first be removed from the image. Morphological closing was used to remove dark details from the image. When the size of the structuring element corresponds to the vessel width in OD, vessels are removed from the image, leaving a lighter background in the region previously occupied by them. Since the blood vessels were determined to be no wider than 14 pixels, we started with a symmetrical disc structuring element of radius 15 pixels. To get a more homogeneous OD region, we used successively larger structuring elements by 10 pixels and performed closing three times. In order to remove the large intensity peaks and make the OD region homogenous after closing, we applied opening by reconstruction with a disc structural element whose radius is 10 pixels larger than the one used in the last closing operation. Since closing is the combination of dilation and erosion with the same structure element, the OD boundary inaccuracy recorded is minor. Opening by reconstruction remove the very bright region smaller than the structural element without altering the papillary region shape.

Fast Hybrid Level set Model

The technique used in this study is based on our previous development of a hybrid level set model to ultrasound cardiac image segmentation [21, 22]. The level set model is given as:

$$\frac{\partial \varphi}{\partial t} = g\varepsilon\kappa|\nabla\varphi| - \left\{(1-s(x,y))\left[\beta_1\left(\left(u(x,y),v(x,y)\right)\cdot\nabla\varphi\right)\right] + s(x,y)\beta_2\nabla g\cdot\nabla\varphi\right\}$$

Where the external forces of the above deformable model are the gradient vector flow (GVF) $\left(u(x,y),v(x,y)\right)$ and the advection vector determined by edge vector ∇g. g is defined as:

$$g(x,y) = \frac{1}{1+\left(\left|\nabla\left(G_\sigma(x,y) * I(x,y)\right)\right|/\gamma\right)^2}$$

The GVF allows the curve has relatively free initialization and quick deformations at the homogenous region at the beginning of deformation. The edge vector field is designed to stop the edge leaking at weak edges when the curve is approaching the true boundaries. The internal force of the model is contour curvature k. $s(x,y)$ is a step function defined as:

$$s(x,y) = \begin{cases} 0, & Ave_{\varphi(x,y,t)=0}\left(f(x,y)\right) < T_{res} \\ 1, & Ave_{\varphi(x,y,t)=0}\left(f(x,y)\right) \geq T_{res} \end{cases}$$

where $f(x,y)$ is the image map function defined by:

$$f(x,y) = \left(\left|\nabla(G_\sigma(x,y) * I(x,y))\right|/\gamma\right)^2$$

The value of $s(x,y)$ is determined by the average of the edge map over the current zero level-set at each iteration.

Since GVF is computationally time consuming, we used region intensity information in the level set model to make the model robust to the segmentation initialization. Meanwhile, it also provides a more powerful stopping function at weak edges. This method is called "fast hybrid level set model". The curve evolution PDE is presented as:

$$\frac{\partial \varphi}{\partial t} = \alpha(I-\lambda)|\nabla\varphi| + g\varepsilon\kappa|\nabla\varphi| - \beta\nabla g\cdot\nabla\varphi$$

The first term on the right hand side represents expansion or contraction movement based on the comparison between the region intensity enclosed by the contour and a predefined threshold λ indicating the lower bound of the target object intensity. Normally, the OD exhibits higher intensities than the rest of the image. If the intensity of the region enclosed by the contour is greater than the threshold, the contour expands along the curve normal direction. Otherwise, it shrinks at the reverse direction of the curve normal. The second term is the internal force determined by curvature. The third term is the edge vector which helps stopping the evolving curve at the object boundary. α, ε, β are the parameters to control the balance of forces.

Zhang [20] used a fast and unconditionally stable finite difference method to solve the above PDE. It is called additive operator splitting (AOS) approach. The above equation can be simplified to

$$\frac{\partial \varphi}{\partial t} = \alpha(I-\lambda) + \beta div\left(g\nabla\varphi\right)$$

if φ is a signed distance function (SDF) defined in level set model, i.e. $|\nabla\varphi| = 1$, and $\varepsilon = \beta$. where, $k = div(\nabla\varphi/|\nabla\varphi|)$. The above PDE equation could be solved efficiently by using the AOS approach.

The threshold λ should be set at the lower bound of OD region intensity. We set the value of λ based on the contrast estimation of the ROI after morphology operations:

$$\lambda = \mu + c\sigma$$

where μ and σ are the mean and standard deviation of the ROI intensity. Since the OD only occupies a small part of ROI, the mean intensity of ROI tends to the intensity of background, we add a coefficient $1 < c < 2$ to make the threshold λ higher to distinguish the OD region intensity from the ROI's background. We choose $\alpha = 10, \beta = 1$ for OD segmentation in retinal images.

Least Square Ellipse Fitting

The curvature is used as an internal force to make the evolving contour smooth during the deformation. The final curve may still appear irregular due to the influence of strong blood vessels. We apply the least square criterion to estimate the best fit to an ellipse from the detected OD boundary. This step can generate smooth OD borders and is useful for optic cup-to-disc ratio computation in glaucoma analysis.

3. RESULTS

3.1 Data set

In this study 1200 digital color fundus photographs were tested. They were collected from a diabetic retinopathy publicly available database kindly provided by the Messidor program partners (see http://messidor.crihan.fr). The database contains 1200 color fundus images of the posterior pole acquired by 3 ophthalmologic departments (400 images from each department) using a color video 3CCD camera on a Topcon TRC NW6 non-mydriatic retinograph with a 45 degree field of view. 800 images were acquired with pupil dilation (one drop of Tropicamide at 10%) and 400 without dilation. The images were captured using 8 bits per color channel at three different image sizes: 1440×960, 2240×1488, or 2304×1536 pixels. The optic disc segmentation "gold standard" images are publicly available and kindly provided by University of Huelva, Spain (http://www.uhu.es/retinopathy) [15]. Fovea location ground truth was provided by an expert ophthalmic technician.

3.2 Optic disc and fovea location

Tables 1 and 2 summarize the results for OD and fovea location. The results in this section were obtained based on the original image resolution. If the detected OD center is within the actual circumference of the optic disc in the gold standard, then it is considered success. For the fovea detection, we determined success if the detected position is within half of the OD radius distance of the marked fovea ground truth.

Table 1 presents the results according to the level of retinopathy as graded by Messidor specialists. Grade 0 means no retinopathy, grades 1 and 2 correspond to patients with non-proliferative retinopathy (NPDR), and grade 3 corresponds to patients with severe NPDR or proliferative DR. Table 2 presents the results according to the risk of macular edema, assessed by the present of exudates in the image. Grade 0 corresponds to normal images (no exudates), grade 1 to images with exudates located more than 1 disc-diameter away from the fovea, and level 2 to images with exudates located within 1 disc-diameter away from the fovea (highest risk of macular edema).

We notice that the images with highest grade of diabetic retinopathy and the risk of macular edema, have the lowest success rate of OD and fovea location. It is interesting that the images with grade 1 of diabetic retinopathy and the risk of macular edema, have the highest success rate. The reason might be a lot of normal images, which have no retinopathy, have myopic crescents, myelinated nerve fibers or peripapillary atrophy, all of which contribute to incorrect results from the algorithm.

Figure 3 shows some examples of the optic disc and fovea location results. The algorithm was implemented in MATLAB v7.11 (MathWorks). The average running time of the optic disc and fovea localization is 3.9 seconds per image (1440×960) on an Intel® Xeon® CPU W3520, 2.67GHz, 6GB RAM computer.

Figure 3, Examples of OD and fovea detection (X represent ground truth, + represent the detected OD and fovea locations). Note that our algorithm disregards the myelinated nerve fibers below the disc in the left image thanks to the complementary use of vessel location within the OD.

Table 1 Diabetic Retinopathy Grade and OD, fovea location results

DIABETIC RETINOPATHY GRADE			
DR Grade	**Number of images**	**Optic Disc Detection**	**Fovea Detection**
3	260	96.16%	85.77%
2	247	99.19%	95.95%
1	153	99.34%	99.35%
0	540	98.71%	97.78%
total	**1200**	**98.33%**	**95%**

Table 2 Risk of Macular Edema and OD, fovea location results

RISK OF MACULAR EDEMA			
ME Grade	**Number of images**	**Optic Disc Detection**	**Fovea Detection**
2	154	97.26%	85.71%
1	75	100%	98.67%
0	971	98.39%	96.19%
total	**1200**	**98.33%**	**95%**

3.3 Optic disc segmentation

The performance of the OD segmentation algorithm is quantitatively evaluated using the mean absolute distance (MAD). MAD measures the average difference between two OD contours, and is obtained by averaging the distance to the closest point (DCP) of all the points on the two curves. If the two curves Γ_1 and Γ_2 can be represented as finite sets of points $\Gamma_1 = \left(n_1, n_2, \cdots, n_p\right)$ and $\Gamma_2 = \left(m_1, m_2, \cdots, m_q\right)$, The DCP for n_i on the curve Γ_1 to the curve Γ_2 is defined as

$$d\left(n_i, \Gamma_2\right) = \min_j \left\| m_j - n_i \right\|.$$

The mean absolute distance (MAD) between the two curves is defined as:

$$M\left(\Gamma_1, \Gamma_2\right) = \frac{1}{2}\left[\frac{1}{p}\sum_{i=1}^{p} d\left(n_i, \Gamma_2\right) + \frac{1}{q}\sum_{j=1}^{q} d\left(m_j, \Gamma_1\right)\right]$$

The Haudorff distance finds the maximum difference between the corresponding points on the two curves. It is defined as the maximum of the DCPs between the two curves:

$$H\left(\Gamma_1, \Gamma_2\right) = \max\left(\max_i\left(d\left(n_i, \Gamma_2\right)\right), \max_j\left(d\left(m_j, \Gamma_1\right)\right)\right)$$

Two examples of OD segmentation and the evaluation metric values are presented in Figure 4. The red channel is used for OD segmentation in the first example (images at the first row in Figure 4). The MAD is 3 pixels and the Hausdroff distance is 10 pixels. The second example used CIElab image for OD segmentation since the red channel is severely saturated. The MAD is 7 pixels and Hausdroff distance is 20 pixels.

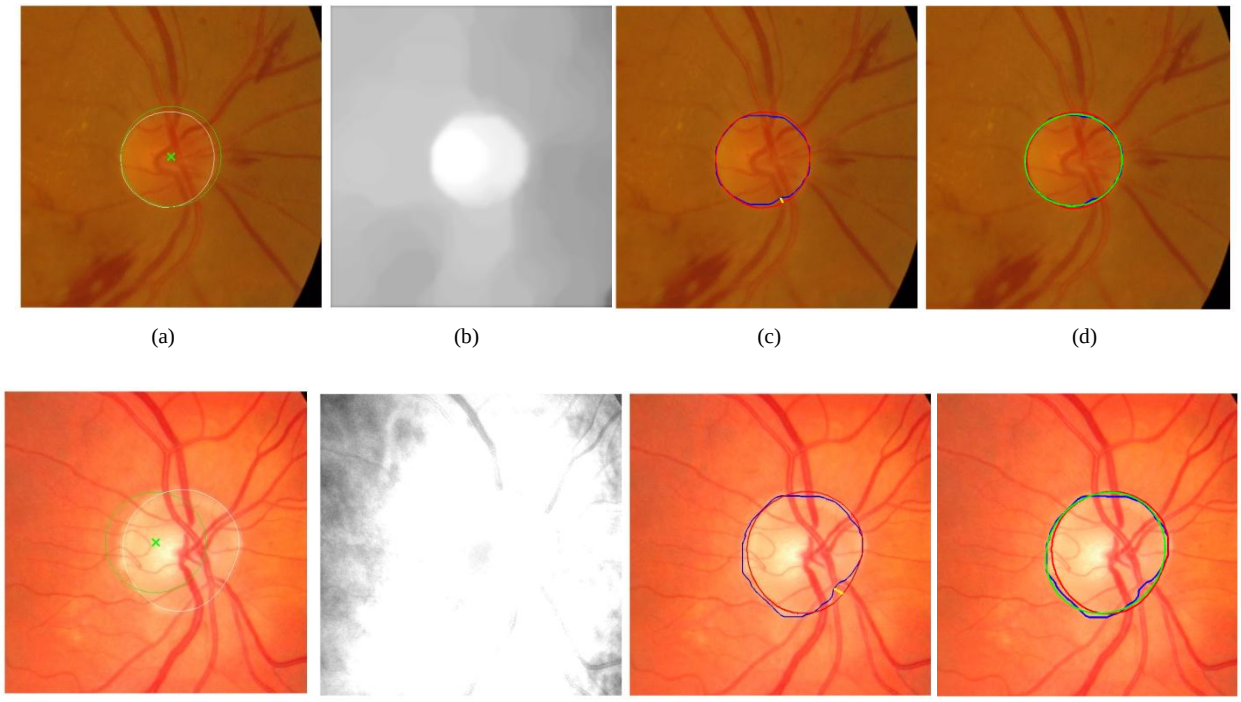

(a) (b) (c) (d)

(e) (f) (g) (h)

Figure 4. (a) A cropped ROI image (OD radius = 100 pixels) with detected OD location and initial contour (green), gold standard in white (b) morphology closing and opening by reconstruction (c) computer generated segmentation in blue, gold standard in red, and Hausdroff distance in yellow.(d) computer generated segmentation in blue, ellipse fitting in green, gold standard in red, MAD = 3 pixels. Hausdroff = 10 pixels. (e) The second example image (OD radius = 100 pixels) with detected OD location and initial contour (green), gold standard in white (f) saturated red channel. (g) computer generated segmentation in blue, gold standard in red, and Hausdroff distance in yellow.(h) computer generated segmentation in blue, ellipse fitting in green, gold standard in red, MAD = 7 pixels. Hausdroff = 20 pixels.

From the quantitative MAD values on Figure 4, we notice that evaluating the algorithm performance in terms of pixels is dependent on the size of the image being analyzed. Instead, we use the ratio between MAD and the estimated OD radius for our algorithm performance evaluation. Table 3 shows the evaluation results on 1200 images in Messidor database without any exclusion for the images with poor image quality. Qualitatively, we define four categories (Excellent, Good, Fair, and Poor) according to the relation between MAD and the OD radius (see Table 3 first column). Fig.5 shows examples in each category. The relation between MAD and OD radius correspond reasonably well to the subjective assessment of segmentation quality.

To evaluate the OD segmentation algorithm independently, OD centers was manually located for the images in which the OD detection fails. It can be observed from Table 3, MAD is less than or equal to one-tenth of OD radius for 66% of 1200 images in the database, which corresponding to the Excellent to Good range. MAD is less than or equal to one-third of OD radius for 97% of the images in the database, which corresponding to the Excellent to Fair range. The average MAD obtained for the whole set of images was about one-tenth (10.5%) of the OD radius regardless the different image resolutions. The average computation time for optic disc segmentation was 5.9 seconds for image (1440×960) on the same machine as OD detection.

Table 3 Segmentation results of the Messidor database

		Lariboisière	CHU de St Etienne	LaTIM - CHU de BREST	Total
		(2240×1488)	(1440×960)	(1440×960, 2304×1536)	
		(r_{OD_img} = 100 pixs)	(r_{OD_img} = 70 pixs)	(r_{OD_img1}=70 pixs, r_{OD_img2}=110 pixs)	
Excellent	MAD ≤ 1/20 × r_{OD_img}	34%	29%	33%	32%
Good	MAD ≤ 1/10× r_{OD_img}	71%	64%	64%	66%
Fair	MAD ≤ 1/5× r_{OD_img}	90%	89%	87%	89%
	MAD ≤ 1/3× r_{OD_img}	98%	98%	96%	97%
Poor	MAD > 1/3× r_{OD_img}	100%	100%	100%	100%
	Mean MAD (pixs)	9.5	7.2	8.2, 11.5	
	Mean MAD / r_{OD_img}	9.50%	10.29%	11.71%, 10.46%	10.49%

(a) (b) (c) (d) (e)

Figure 5. (a) Segmentation examples for OD radius = 100 pixels. Computer generated segmentation in blue, ellipse fitting in green, gold standard in red. (a) Excellent, MAD = 3.3 pixels (b) Good, MAD = 8.2 pixels (c) Fair, MAD = 17.4 pixels. (d) Fair, MAD = 25.1 pixels. (e) Poor, MAD = 93.4 pixels

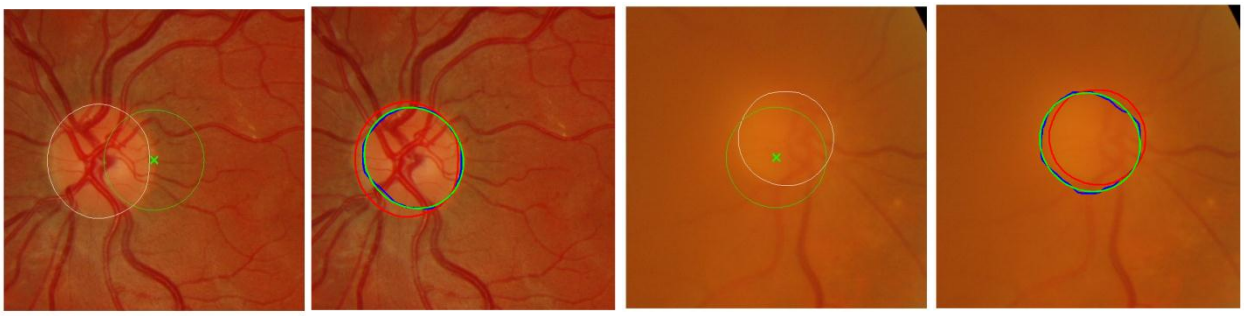

(a) (b) (c) (d)

Figure 6. (a) the OD location is out of OD boundary in the gold standard (white contour), initial contour is green (OD radius = 100 pixels), (b) computer generated segmentation in blue, ellipse fitting in green, gold standard in red. MAD = 11 pixels. Hausdroff = 30 pixels. (c) Very blurred OD boundary with initialization (green), gold standard in white. (d) computer generated segmentation in blue, ellipse fitting in green, gold standard in red. MAD = 12 pixels. Hausdroff = 23 pixels.

In some cases, the automatically initialized contour intersected the optic disc boundary due to the offset between the located OD and true OD center (within one disc radius). The fast hybrid level set method has the ability to drive the contour to enclose the regions with intensity greater than certain value even the initialization is not "perfect". In Figure 6(a), the detected OD location is out of the OD boundary in the gold standard. Even then, the level set model still converges to the true OD border (Figure6 (b)). This shows that the segmentation method is robust to the variations in detected OD locations. The algorithm also performs well on the OD with blurred margin due to cataracts (Figure6 (c)). The region intensity information in the hybrid model forces the evolving contour converges to the true OD boundary as shown in Figure 6(d).

4. DISCUSSION

To compare to the results obtained by Aquino et. al. [15], we also compute the overlapping degree between the segmented OD areas A_s and the true OD regions A_t marked in gold standard images, which defined as:

$$R = \frac{A_s \cap A_t}{A_s \cup A_t}$$

The average area overlap ratio between the segmented OD boundary and the gold standard for the whole dataset is 83%, which is 3% less than the one obtained by Aquino et. al. This result might due to the following possible reasons: First, The gold standard of OD boundary on each image in the Messidor database was created by single grader from Aquino's research group since the database is huge. That means that a certain inter-reader variability is to be expected. Second, they down-sampled all the images to 640×640 for OD segmentation, thus reducing the image resolution up to about 10 times compared to the original images. After OD segmentation, the images were up-sampled to the original image size to compare to the gold standard marked on the original images. This down- and up-sampling procedure definitely introduces some uncertainty in the final results, but benefits the computation speed. Our algorithm uses the detected OD location as the center of the region of interest (ROI), the size of ROI depend on the automatically determined OD radius based on the field of view of camera and image resolution. No extra uncertainty or errors was introduced during OD segmentation and evaluation.

Our deformable model is sensitive to the peripapillary atrophy and myelinated nerve fibers which appear very bright region and are connected to the OD border (see Figure 5 (e) as an example). Another common case of poor segmentation is that when the image has very low contrast OD boundary companied with very strong vessel branches, after the vessel removal by morphology operations, the brightness of OD and contrast of OD border was further decreased, the poor OD segmentation result is inevitable. Further improvement could be implemented by removing vessels without decreasing the OD boundary contrast using vessel masks.

The hybrid level set deformable model has the potential to adapt to any topological change of the target object. Therefore, it is sensitive to irregular and non-homogeneousness of the target object. we used least square ellipse fitting to smooth the irregular segmented OD boundary and prepare for optic cup-to-disc ratio computation in future glaucoma analysis. We noticed that there is no significant difference for average MAD and area overlapping ratio with or without ellipse fitting after level set segmentation; meanwhile, there is a significant difference for Hausdroff distance with or without ellipse fitting. The average Hausdroff distance is reduced by one-tenth of the original value after ellipse fitting.

5. CONCLUSION

A new, robust OD and fovea localization methodology for fast retinal image screening has been developed. The OD detection methodology not only exploits the appearance features of the OD, but also the vessels location and orientation inside the OD to increase robustness. The OD segmentation method uses both the region information and object boundary with simple initialization to achieve robust, fast, and accurate segmentation. The future DR screening system will have to be robust, provide high accuracy rates, and be fast in order to support high workloads and near real time operation. The methodology developed here has been designed to satisfy those requirements. The robustness and efficiency makes the methodology suitable for assisting on automatic screening for early signs of diabetic retinopathy.

REFERENCES

[1] Winder, R. J., Morrow,P. J., McRitchie,I. N., Bailie,J. R. and Hart,P. M.,"Algorithms for digital image processing in diabetic retinopathy," Computerized Medical Imaging and Graphics, 33(8),608-622 (2009).

[2] Youssif, A., Ghalwash, A. Z., and Ghoneim, A., "Optic disc detection from normalized digital fundus images by means of a vessels' direction matched filter," Ieee Transactions on Medical Imaging, 27(1), 11-18 (2008).

[3] Osareh, A.,Mirmehdi,M., Thomas,B. and Markham R.,"Comparison of Colour Spaces for Optic Disc Localisation in Retinal Images," In Proceedings of the 16 th International Conference on Pattern Recognition (ICPR'02), 1,10743-10746 (2002).

[4] Lalonde, M., Beaulieu, M., and Gagnon, L.,"Fast and robust optic disc detection using pyramidal decomposition and Hausdorff-based template matching," Ieee Transactions on Medical Imaging, 20, 1193-1200 (2001).

[5] Lowell, J.,Hunter,A., Steel,D., Basu,A., Ryder,R., Fletcher,E. and Kennedy,L.,"Optic nerve head segmentation," Ieee Transactions on Medical Imaging 23(2), 256-264 (2004).

[6] Tobin, K. W., Chaum,E., Govindasamy, V. P. and Karnowski,T. P., "Detection of anatomic structures in human retinal imagery," Ieee Transactions on Medical Imaging 26(12), 1729-1739 (2007).

[7] Niemeijer, M., Abramoff, M. D., and van Ginneken, B.,"Fast detection of the optic disc and fovea in color fundus photographs," Medical Image Analysis 13(6), 859-870 (2009).

[8] Fleming, A. D., Goatman, K. A., Philip, S., Olson,J. A. and Sharp,P. F.,"Automatic detection of retinal anatomy to assist diabetic retinopathy screening," Physics in Medicine and Biology 52(2), 331-345 (2007).

[9] Niemeijer, M., Abramoff, M. D., and van Ginneken, B.,"Segmentation of the optic disc, macula and vascular arch in fundus photographs," Ieee Transactions on Medical Imaging 26(1),116-127 (2007).

[10] Hoover, A., and Goldbaum, M.,"Locating the optic nerve in a retinal image using the fuzzy convergence of the blood vessels," Ieee Transactions on Medical Imaging, 22(8), 951-958 (2003).

[11] Foracchia, M., Grisan, E., and Ruggeri, A.,"Detection of optic disc in retinal images by means of a geometrical model of vessel structure," Ieee Transactions on Medical Imaging 23(10), 1189-1195 (2004).

[12] Mendels, F., heneghan, C., and Thiran, J. P.,"Identification of the optic disk boundary in retinal images using active contours," Proceedings of the Irish Machine Vision and Image Processing Conference, 103-115 (1999)

[13] Li, H. Q., and Chutatape, O.,"Automated feature extraction in color retinal images by a model based approach," Ieee Transactions on Biomedical Engineering, 51(2), 246-254 (2004).

[14] Xu, J., Chutatape,O., Sung,E.,Zheng, C., and Kuan,P. C. T., "Optic disk feature extraction via modified deformable model technique for glaucoma analysis," Pattern Recognition, 40(7), 2063-2076 (2007).

[15] Aquino, A., Gegundez-Arias, M. E., and Marin, D.,"Detecting the Optic Disc Boundary in Digital Fundus Images Using Morphological, Edge Detection, and Feature Extraction Techniques," Ieee Transactions on Medical Imaging, 29(11), 1860-1869 (2010).

[16] "http://www.optos.com/en-us/Professionals/Optometry/Case-Clinical-Studies/".

[17] Hubbard, L. D., Brothers,R. J., King,W. N., Clegg,L. X., Klein, R., Cooper,L. S.,Sharrett, A. R.,Davis, M. D. and Cai,J. W.,"Methods for evaluation of retinal microvascular abnormalities associated with hypertension/sclerosis in the atherosclerosis risk in communities study," Ophthalmology, 106, 2269-2280 (1999).

[18] Chaudhuri, S., Chatterjee, S., Katz,N., Nelson,M. and Goldbaum, M. ,"Detection of Blood-Vessels in Retinal Images Using Two-Dimensional Matched-Filters," Ieee Transactions on Medical Imaging, 8(3), 263-269 (1989).

[19] Cunningham, D. J., Cunningham's Text-Book of Anatomy, Oxford Univ. Press, New York, (1981).

[20] Zhang, Y., Matuszewski,B. J., Shark, L.K. and Moore, C. J.,"Medical Image Segmentation Using New Hybrid Level-Set Method," Proceedings of the 2008 Fifth International Conference BioMedical Visualization, 71-76 (2008).

[21] Yu, H., Pattichis, M. S., and Goens, M. B.,"Multi-view 3D Reconstruction with Volumetric Registration in a Freehand Ultrasound Imaging System," Proc. of the SPIE International Symposium on Medical Imaging, 6147(6), 45-56 (2006).

[22] Yu, H., Pattichis, M. S., and Goens, M. B.," Robust Segmentation of Freehand Ultrasound Image Slices Using Gradient Vector Flow Fast Geometric Active Contours," Proc. of the 2006 IEEE Southwest Symposium on Image Analysis and Interpretation, 115-119 (2006).